Closing the loop as an inverse problem: the real-time control of THEMIS adaptive optics

Éric Thiébaut, Michel Tallon, Isabelle Tallon-Bosc, Bernard Gelly, Richard Douet, Maud Langlois, Gil Moretto

Closing the loop as an inverse problem: the real-time control of Themis adaptive optics

Éric Thiébaut[a], Michel Tallon[a], Isabelle Tallon-Bosc[a], Bernard Gelly[b], Richard Douet[b], Maud Langlois[a], and Gil Moretto[b]

[a]Univ. Lyon, Univ. Lyon 1, ENS de Lyon, CNRS, Centre de Recherche Astrophysique de Lyon UMR5574, F-69230, Saint-Genis-Laval, France
[b]CNRS IRL20009 FSLAC, 38205 Laguna, Tenerife, Spain

ABSTRACT

We have taken advantage of the implementation of an adaptive optics system on the Themis solar telescope to implement innovative strategies based on an inverse problem formulation for the control loop. Such an approach encompassing the whole system implies the estimation of the pixel variances of the Shack-Hartmann wavefront sensor, a novel real-time method to extract the wavefront slopes as well as their associated noise covariance, and the computation of pseudo-open loop data. The optimal commands are computed by iteratively solving a regularized inverse problem with spatio-temporal constraints including Kolmogorov statistics. The latency of the dedicated real-time control software with conventional CPU is shorter than 300 µs from the acquisition of the raw 400×400 pixel wavefront sensor image to the sending of the commands.

Keywords: solar adaptive optics, inverse problems framework, real-time control, iterative methods, sufficient statistic, pseudo-open loop

1. OUTLINE

The Themis solar telescope has been equipped with an adaptive optics (AO) system comprising a 92-actuator Alpao deformable mirror (DM) and a 10×10 Shack-Hartmann wavefront sensor (SH-WFS) operated at 1 kHz (see Figure 1). Developing the real-time control (RTC) of this AO system was the opportunity to implement innovative strategies studied in our team for a decade[1–4] and all based on an inverse problem formulation of the estimation of the commands applied to the DM. The inverse problem approach is known to yield excellent estimators which optimally combine all available information but is usually not fully used for real-time systems because of the computational burden and of the amount of required information (e.g., all covariance matrices must be provided). Since sufficient statistics are required at all processing stages, we developed specific detector calibration and pre-processing procedures to compensate for the non-uniformity of the WFS detector response and optical throughput and to yield estimated pixel variances.[5] We also developed a novel method to extract, in real-time, the wavefront slopes and the covariance matrix of their noise from the images of the WFS despite the very low contrast and the temporal evolution of the structures at the Sun's surface.[5] For the control, the chosen approach leads to work with pseudo-open loop data, which requires a good model of the so-called interaction matrix of the system. This matrix is calibrated by measuring the effects of sending stochastic commands (Section 3). The optimal commands are eventually estimated by iteratively solving a regularized inverse problem (Section 2). Various spatio-temporal constraints are implemented including a priori Kolmogorov covariance for the wavefront. The dedicated RTC is implemented on a 4-core conventional CPU running under Linux and is able to close the loop even in harsh conditions with a latency shorter than 300 µs from the acquisition of the raw 400×400 pixel WFS image to the sending of the commands (Section 4).

2. OPTIMAL CONTROL

An adaptive optics (AO) system consists in a wavefront sensor (WFS), a deformable mirror (DM), and real time control (RTC) hardware and software to compute and send the commands for the actuators of the DM given the measurements of the WFS. In this section, we aim at deriving optimal control commands for the AO system under clearly specified assumptions.

Further author information: E-mail: eric.thiebaut@univ-lyon1.fr

Themis solar telescope
Tenerife, Canaria Islands
Ø 90 cm, altitude 2400 m

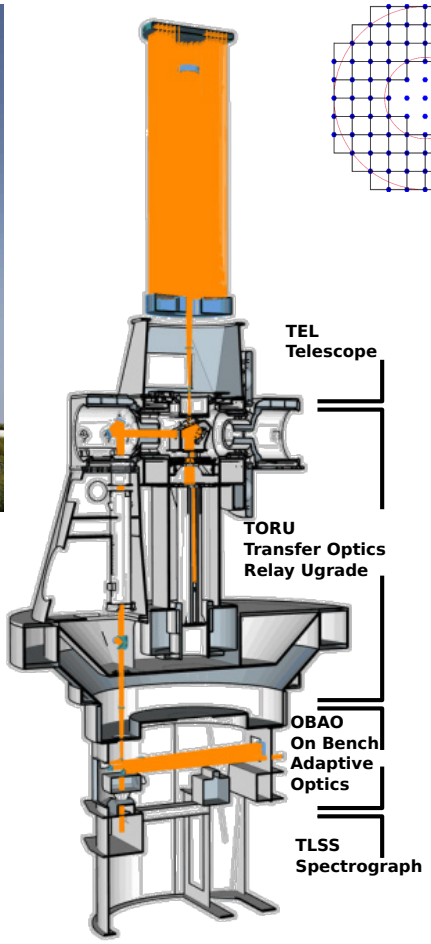

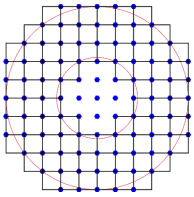

Themis AO system
76 subapertures (10×10)
97 actuators (11×11, Alpao)
RTC ≥1 kHz

Wavefront sensor at the telescope

Figure 1. The Themis AO system. Left: outside view of the Themis telescope. Center: optical layout of the telescope with the AO system and the spectrograph. Top: layout of the sub-pupils of the Shack-Hartmann wavefront sensor and of the actuators of the deformable mirror. Right: the wavefront (camera and optics).

2.1 Model of the Wavefront Sensor Data

At each time frame t, the wavefront sensor delivers data $\boldsymbol{d}_t \in \mathbb{R}^{n_{\mathrm{dat}}}$ whose linearized model writes:

$$\boldsymbol{d}_t = \boldsymbol{S} \cdot (\boldsymbol{w}_t + \boldsymbol{M} \cdot \boldsymbol{a}_t) + \boldsymbol{z}_t \tag{1}$$

where $\boldsymbol{S} \in \mathbb{R}^{n_{\mathrm{dat}} \times n_{\mathrm{wav}}}$ is the linear response matrix of the sensor, $\boldsymbol{w}_t \in \mathbb{R}^{n_{\mathrm{wav}}}$ is the wavefront during the exposure of frame t, $\boldsymbol{M} \in \mathbb{R}^{n_{\mathrm{wav}} \times n_{\mathrm{act}}}$ is the linear response matrix of the deformable mirror, the so-called *influence matrix*, $\boldsymbol{a}_t \in \mathbb{R}^{n_{\mathrm{act}}}$ is the vector of actuators commands during this frame, and $\boldsymbol{z}_t \in \mathbb{R}^{n_{\mathrm{dat}}}$ accounts the contribution of the noise. Here n_{dat} is the number of measurements per frame, n_{act} is the number of actuators, and n_{wav} is the size of the wavefront $\boldsymbol{w}_t$ which can be arbitrarily large even though it is finite in practice. For a Shack-Hartmann wavefront sensor, the measurements are the wavefront slopes for each sub-pupil, hence $n_{\mathrm{dat}} = 2\, n_{\mathrm{sub}}$ with n_{sub} the number of sub-pupils.

In what follows and for the sake of simplicity, we assume that the mirror linear response $\boldsymbol{M}$ and the wavefront sensor linear response $\boldsymbol{S}$ are stable in time. This can be easily relaxed by adding a subscript t for these matrices.

2.2 Optimal Commands

At any time frame t, the best commands are those that will minimize the residual wavefront aberrations $\boldsymbol{w}_{t+\delta t} + \boldsymbol{M} \cdot \boldsymbol{a}_{t+\delta t}$ at frame $t + \delta t$ where $\delta t > 0$ is the time delay (in number of frames) for the wavefront sensor to effectively *see* the effects of given actuators commands. For example, to maximize the Strehl we would like to apply the following commands:

$$\boldsymbol{a}_{t+\delta t} = \arg\min_{\boldsymbol{a}} \left\langle \|\boldsymbol{w}_{t+\delta t} + \boldsymbol{M} \cdot \boldsymbol{a}\|^2 \,\middle|\, \boldsymbol{\theta}_t \right\rangle \tag{2}$$

where $\boldsymbol{\theta}_t$ represents known information at time t and $\langle \boldsymbol{x} \,|\, \boldsymbol{\theta} \rangle$ denotes the conditional expectation of $\boldsymbol{x}$ knowing $\boldsymbol{\theta}$. In other words, we want to reduce as much as possible the residuals on the mean at time $t + \delta t$ by exploiting all available information at time t. Thanks to taking the expectation of the residual errors, only the statistics*, not the actual realization, of the future wavefront $\boldsymbol{w}_{t+\delta t}$ need to be known and the above problem has a closed form solution:

$$\boldsymbol{a}_{t+\delta t} = -\boldsymbol{M}^{\dagger} \cdot \overline{\boldsymbol{w}}_{t+\delta t|t}, \tag{3}$$

where $\boldsymbol{M}^{\dagger} = \left(\boldsymbol{M}^{\top} \cdot \boldsymbol{M}\right)^{-1} \cdot \boldsymbol{M}^{\top}$ is the pseudo inverse of $\boldsymbol{M}$, the linear response of the deformable mirror, and $\overline{\boldsymbol{w}}_{t+\delta t|t} = \left\langle \boldsymbol{w}_{t+\delta t} \,\middle|\, \boldsymbol{\theta}_t \right\rangle$ is the expectation of the wavefront at time $t + \delta t$ knowing information available at time t. This apparently simple solution turns out to be quite challenging to compute in a real-time system. We develop in what follows the equations leading to $\overline{\boldsymbol{w}}_{t+\delta t|t}$ with as few assumptions as possible to remain general.

2.3 Known Information and Pseudo Open-Loop Data

At every time frame t, new information is brought by the wavefront sensor data $\boldsymbol{d}_t$ and by the corresponding commands $\boldsymbol{a}_t$. Hence $\boldsymbol{\theta}_t = \boldsymbol{\theta}_{t-1} \cup \{\boldsymbol{d}_t, \boldsymbol{a}_t\}$ expresses the information gain between frames $t-1$ and t and is to be used with Eq. (1). It is however equivalent and simpler to consider the pseudo open-loop[6] (POL) data instead:

$$\boldsymbol{y}_t = \boldsymbol{d}_t - \boldsymbol{G} \cdot \boldsymbol{a}_t = \boldsymbol{S} \cdot \boldsymbol{w}_t + \boldsymbol{z}_t \tag{4}$$

where $\boldsymbol{G} = \boldsymbol{S} \cdot \boldsymbol{M}$ is the so-called *interaction matrix*. Then, the updating rule for the available information is just:

$$\boldsymbol{\theta}_t = \boldsymbol{\theta}_{t-1} \cup \{\boldsymbol{y}_t\}. \tag{5}$$

Thanks to this change of variables, the commands will not explicitly appear in the equations leading to $\overline{\boldsymbol{w}}_{t+\delta t|t}$.

*in fact, just the first and second moments

2.4 Updating Rules

Equation (3) readily shows that obtaining the best commands is a matter of being able to predict the expected shape of the wavefront in a near future. The wavefronts at different times certainly come into play in the problem and, to be as general as possible, we consider the spatio-temporal wavefront $\boldsymbol{x}$ which is the concatenation of the wavefronts in all (future, current, and past) temporal frames:

$$\boldsymbol{x} = \begin{pmatrix} \cdots & \boldsymbol{w}_{t-2}^\top & \boldsymbol{w}_{t-1}^\top & \boldsymbol{w}_t^\top & \boldsymbol{w}_{t+1}^\top & \boldsymbol{w}_{t+2}^\top & \cdots \end{pmatrix}^\top . \tag{6}$$

From Eq. (4), the spatio-temporal wavefront $\boldsymbol{x}$ is related to the pseudo open-loop data $\boldsymbol{y}_t$ in the t-th frame by:

$$\boldsymbol{y}_t = \boldsymbol{H}_t \cdot \boldsymbol{x} + \boldsymbol{z}_t, \tag{7}$$

where $\boldsymbol{H}_t$, the extended linear model matrix of the data, has the following block structure with blocks of size $n_{\text{dat}} \times n_{\text{wav}}$:

$$\boldsymbol{H}_t = \begin{pmatrix} \cdots & \boldsymbol{0} & \boldsymbol{0} & \boldsymbol{S} & \boldsymbol{0} & \boldsymbol{0} & \cdots \\ \cdots & t-2 & t-1 & t & t+1 & t+2 & \cdots \end{pmatrix}. \tag{8}$$

At arrival of data frame t, the *maximum a posteriori* (MAP) estimator of $\boldsymbol{x}$ can be expressed as:

$$\begin{aligned}
\boldsymbol{x}_{|t} &\overset{\text{def}}{=} \arg\max_{\boldsymbol{x}} \Pr\big(\boldsymbol{x} \,\big|\, \boldsymbol{\theta}_t\big) && && (9)\\
&= \arg\max_{\boldsymbol{x}} \Pr\big(\boldsymbol{x} \,\big|\, \boldsymbol{y}_t, \boldsymbol{\theta}_{t-1}\big) && \text{(since } \boldsymbol{\theta}_t = \boldsymbol{\theta}_{t-1} \cup \{\boldsymbol{y}_t\}\text{)} && (10)\\
&= \arg\max_{\boldsymbol{x}} \Pr\big(\boldsymbol{x}, \boldsymbol{y}_t \,\big|\, \boldsymbol{\theta}_{t-1}\big) && \text{(by Bayes' rule and as } \Pr\big(\boldsymbol{y}_t \,\big|\, \boldsymbol{\theta}_{t-1}\big) \text{ is constant in } \boldsymbol{x}\text{)} && (11)\\
&= \arg\max_{\boldsymbol{x}} \Pr\big(\boldsymbol{y}_t \,\big|\, \boldsymbol{x}, \boldsymbol{\theta}_{t-1}\big)\ \Pr\big(\boldsymbol{x} \,\big|\, \boldsymbol{\theta}_{t-1}\big) && \text{(again by Bayes' rule).} && (12)
\end{aligned}$$

For an AO system, the noise and the wavefronts are independent and the noise terms in two different frames are mutually independent. As a consequence, the pseudo open-loop data $\boldsymbol{y}_t$ only depend on the wavefront $\boldsymbol{w}_t$ and thus $\Pr\big(\boldsymbol{y}_t \,\big|\, \boldsymbol{x}, \boldsymbol{\theta}_{t-1}\big) = \Pr\big(\boldsymbol{y}_t \,\big|\, \boldsymbol{x}\big)$. The conditional expectation and covariance of the pseudo open-loop data can then be derived as follows:

$$\begin{aligned}
\langle \boldsymbol{y}_t \,|\, \boldsymbol{x} \rangle &= \langle \boldsymbol{H}_t \cdot \boldsymbol{x} + \boldsymbol{z}_t \,|\, \boldsymbol{x} \rangle && \text{(from Eq. (7))}\\
&= \boldsymbol{H}_t \cdot \boldsymbol{x} + \langle \boldsymbol{z}_t \,|\, \boldsymbol{x} \rangle && \text{(by linearity of the expectation)}\\
&= \boldsymbol{H}_t \cdot \boldsymbol{x}, && && (13)
\end{aligned}$$

the latter assuming the noise is centered in the sense that $\langle \boldsymbol{z}_t \,|\, \boldsymbol{x} \rangle = \boldsymbol{0}$[†], and:

$$\begin{aligned}
\operatorname{Cov}(\boldsymbol{y}_t \,|\, \boldsymbol{x}) &= \operatorname{Cov}(\boldsymbol{H}_t \cdot \boldsymbol{x} + \boldsymbol{z}_t \,|\, \boldsymbol{x}) && \text{(from Eq. (7))}\\
&= \boldsymbol{H}_t \cdot \operatorname{Cov}(\boldsymbol{x} \,|\, \boldsymbol{x}) \cdot \boldsymbol{H}_t^\top + \operatorname{Cov}(\boldsymbol{z}_t \,|\, \boldsymbol{x}) && (\boldsymbol{x} \text{ and } \boldsymbol{z}_t \text{ mutually independent})\\
&= \operatorname{Cov}(\boldsymbol{z}_t) && \text{(idem and since } \operatorname{Cov}(\boldsymbol{x} \,|\, \boldsymbol{x}) = \boldsymbol{0}\text{).} && (14)
\end{aligned}$$

Assuming Gaussian statistics for all variables, then yields:

$$\boldsymbol{x}_{|t} = \arg\min_{\boldsymbol{x}} \Big\{ \|\boldsymbol{y}_t - \boldsymbol{H}_t \cdot \boldsymbol{x}\|^2_{\operatorname{Cov}(\boldsymbol{z}_t)^{-1}} + \big\|\boldsymbol{x} - \overline{\boldsymbol{x}}_{|t-1}\big\|^2_{\operatorname{Cov}(\boldsymbol{x} \,|\, \boldsymbol{\theta}_{t-1})^{-1}} \Big\} \tag{15}$$

where $\overline{\boldsymbol{x}}_{|t-1} \overset{\text{def}}{=} \langle \boldsymbol{x} \,|\, \boldsymbol{\theta}_{t-1} \rangle$ and $\operatorname{Cov}(\boldsymbol{x} \,|\, \boldsymbol{\theta}_{t-1})$ are the expectation and the covariance of $\boldsymbol{x}$ knowing $\boldsymbol{\theta}_{t-1}$ and where $\operatorname{Cov}(\boldsymbol{z}_t)$ is the covariance of the noise. This optimization problem is quadratic in $\boldsymbol{x}$ and has a closed form solution:

$$\begin{aligned}
\boldsymbol{x}_{|t} &= \big(\boldsymbol{H}_t^\top \cdot \operatorname{Cov}(\boldsymbol{z}_t)^{-1} \cdot \boldsymbol{H}_t + \operatorname{Cov}(\boldsymbol{x} \,|\, \boldsymbol{\theta}_{t-1})^{-1}\big)^{-1} \cdot \big(\boldsymbol{H}_t^\top \cdot \operatorname{Cov}(\boldsymbol{z}_t)^{-1} \cdot \boldsymbol{y}_t + \operatorname{Cov}(\boldsymbol{x} \,|\, \boldsymbol{\theta}_{t-1})^{-1} \cdot \overline{\boldsymbol{x}}_{|t-1}\big)\\
&= \overline{\boldsymbol{x}}_{|t-1} + \big(\boldsymbol{H}_t^\top \cdot \operatorname{Cov}(\boldsymbol{z}_t)^{-1} \cdot \boldsymbol{H}_t + \operatorname{Cov}(\boldsymbol{x} \,|\, \boldsymbol{\theta}_{t-1})^{-1}\big)^{-1} \cdot \boldsymbol{H}_t^\top \cdot \operatorname{Cov}(\boldsymbol{z}_t)^{-1} \cdot \big(\boldsymbol{y}_t - \boldsymbol{H}_t \cdot \overline{\boldsymbol{x}}_{|t-1}\big) \qquad (16)
\end{aligned}$$

[†]note that $\langle \boldsymbol{z}_t \,|\, \boldsymbol{x} \rangle = \boldsymbol{0} \Longrightarrow \langle \boldsymbol{z}_t \rangle = \boldsymbol{0}$

by simple algebra. Now, using a well known matrix identity,[1,7] we may write:

$$\boldsymbol{x}_{|t} = \overline{\boldsymbol{x}}_{|t-1} + \mathrm{Cov}(\boldsymbol{x} \,|\, \boldsymbol{\theta}_{t-1}) \cdot \boldsymbol{H}_t^\top \cdot \big(\mathrm{Cov}(\boldsymbol{z}_t) + \boldsymbol{H}_t \cdot \mathrm{Cov}(\boldsymbol{x} \,|\, \boldsymbol{\theta}_{t-1}) \cdot \boldsymbol{H}_t^\top\big)^{-1} \cdot \big(\boldsymbol{y}_t - \boldsymbol{H}_t \cdot \overline{\boldsymbol{x}}_{|t-1}\big). \tag{17}$$

Owing to the particular structure of $\boldsymbol{x}$ and of $\boldsymbol{H}_t$, see Eqs. (6) and (8), a few simplifications can be done:

$$\boldsymbol{H}_t \cdot \overline{\boldsymbol{x}}_{|t-1} = \boldsymbol{S} \cdot \overline{\boldsymbol{w}}_{t|t-1}, \tag{18}$$

$$\boldsymbol{H}_t \cdot \mathrm{Cov}(\boldsymbol{x} \,|\, \boldsymbol{\theta}_{t-1}) \cdot \boldsymbol{H}_t^\top = \boldsymbol{S} \cdot \mathrm{Cov}(\boldsymbol{w}_t \,|\, \boldsymbol{\theta}_{t-1}) \cdot \boldsymbol{S}^\top, \tag{19}$$

with $\overline{\boldsymbol{w}}_{t|t-1} \overset{\text{def}}{=} \langle \boldsymbol{w}_t \,|\, \boldsymbol{\theta}_{t-1} \rangle$ and $\mathrm{Cov}(\boldsymbol{w}_t \,|\, \boldsymbol{\theta}_{t-1})$ the expectation and covariance of $\boldsymbol{w}_t$ knowing $\boldsymbol{\theta}_{t-1}$. Introducing:

$$\boldsymbol{Q}_{t|t-1} = \begin{pmatrix} \cdots & \mathbf{0} & \mathbf{0} & \mathrm{Cov}(\boldsymbol{w}_t \,|\, \boldsymbol{\theta}_{t-1})^{-1} & \mathbf{0} & \mathbf{0} & \cdots \\ \cdots & t-2 & t-1 & t & t+1 & t+2 & \cdots \end{pmatrix}, \tag{20}$$

it is possible to write $\boldsymbol{H}_t = \boldsymbol{S} \cdot \mathrm{Cov}(\boldsymbol{w}_t \,|\, \boldsymbol{\theta}_{t-1}) \cdot \boldsymbol{Q}_{t|t-1}$ and putting all together, we obtain:

$$\begin{aligned} \boldsymbol{x}_{|t} &= \overline{\boldsymbol{x}}_{|t-1} + \mathrm{Cov}(\boldsymbol{x} \,|\, \boldsymbol{\theta}_{t-1}) \cdot \boldsymbol{Q}_{t|t-1}^\top \cdot \mathrm{Cov}(\boldsymbol{w}_t \,|\, \boldsymbol{\theta}_{t-1}) \cdot \boldsymbol{S}^\top \cdot \big(\mathrm{Cov}(\boldsymbol{z}_t) + \boldsymbol{S} \cdot \mathrm{Cov}(\boldsymbol{w}_t \,|\, \boldsymbol{\theta}_{t-1}) \cdot \boldsymbol{S}^\top\big)^{-1} \cdot \big(\boldsymbol{y}_t - \boldsymbol{S} \cdot \overline{\boldsymbol{w}}_{t|t-1}\big) \\ &= \overline{\boldsymbol{x}}_{|t-1} + \mathrm{Cov}(\boldsymbol{x} \,|\, \boldsymbol{\theta}_{t-1}) \cdot \boldsymbol{Q}_{t|t-1}^\top \cdot \big(\boldsymbol{w}_{t|t} - \overline{\boldsymbol{w}}_{t|t-1}\big) \end{aligned} \tag{21}$$

where $\boldsymbol{w}_{t|t}$ is the MAP estimator of $\boldsymbol{w}_t$ knowing $\boldsymbol{\theta}_t$. This can be proven using the same rules as before:

$$\begin{aligned} \boldsymbol{w}_{t|t} &\overset{\text{def}}{=} \arg\max_{\boldsymbol{w}_t} \Pr\big(\boldsymbol{w}_t \,\big|\, \boldsymbol{\theta}_t\big) \\ &= \arg\max_{\boldsymbol{w}_t} \Pr\big(\boldsymbol{w}_t, \boldsymbol{y}_t \,\big|\, \boldsymbol{\theta}_{t-1}\big) \\ &= \arg\min_{\boldsymbol{w}_t} \Big\{ \|\boldsymbol{y}_t - \boldsymbol{S} \cdot \boldsymbol{w}_t\|^2_{\mathrm{Cov}(\boldsymbol{z}_t)^{-1}} + \big\|\boldsymbol{w}_t - \overline{\boldsymbol{w}}_{t|t-1}\big\|^2_{\mathrm{Cov}(\boldsymbol{w}_t \,|\, \boldsymbol{\theta}_{t-1})^{-1}} \Big\} \\ &= \big(\boldsymbol{S}^\top \cdot \mathrm{Cov}(\boldsymbol{z}_t)^{-1} \cdot \boldsymbol{S} + \mathrm{Cov}(\boldsymbol{w}_t \,|\, \boldsymbol{\theta}_{t-1})^{-1}\big)^{-1} \cdot \big(\boldsymbol{S}^\top \cdot \mathrm{Cov}(\boldsymbol{z}_t)^{-1} \cdot \boldsymbol{y}_t + \mathrm{Cov}(\boldsymbol{w}_t \,|\, \boldsymbol{\theta}_{t-1})^{-1} \cdot \overline{\boldsymbol{w}}_{t|t-1}\big) \\ &= \overline{\boldsymbol{w}}_{t|t-1} + \big(\boldsymbol{S}^\top \cdot \mathrm{Cov}(\boldsymbol{z}_t)^{-1} \cdot \boldsymbol{S} + \mathrm{Cov}(\boldsymbol{w}_t \,|\, \boldsymbol{\theta}_{t-1})^{-1}\big)^{-1} \cdot \boldsymbol{S}^\top \cdot \mathrm{Cov}(\boldsymbol{z}_t)^{-1} \cdot \big(\boldsymbol{y}_t - \boldsymbol{S} \cdot \overline{\boldsymbol{w}}_{t|t-1}\big) \\ &= \overline{\boldsymbol{w}}_{t|t-1} + \mathrm{Cov}(\boldsymbol{w}_t \,|\, \boldsymbol{\theta}_{t-1}) \cdot \boldsymbol{S}^\top \cdot \big(\mathrm{Cov}(\boldsymbol{z}_t) + \boldsymbol{S} \cdot \mathrm{Cov}(\boldsymbol{w}_t \,|\, \boldsymbol{\theta}_{t-1}) \cdot \boldsymbol{S}^\top\big)^{-1} \cdot \big(\boldsymbol{y}_t - \boldsymbol{S} \cdot \overline{\boldsymbol{w}}_{t|t-1}\big). \quad \blacksquare \end{aligned} \tag{22}$$

The MAP estimator $\boldsymbol{w}_{t|t}$ linearly depends on the noise and the wavefront which are Gaussian variables. It follows that $\boldsymbol{w}_{t|t}$ is also Gaussian, moreover the MAP estimator is equal to the posterior mean and the associated conditional covariance $\mathrm{Cov}(\boldsymbol{w}_t \,|\, \boldsymbol{\theta}_t)$ has a closed form expression:[7]

$$\boldsymbol{w}_{t|t} = \langle \boldsymbol{w}_t \,|\, \boldsymbol{\theta}_t \rangle = \overline{\boldsymbol{w}}_{t|t}, \tag{23}$$

$$\mathrm{Cov}(\boldsymbol{w}_t \,|\, \boldsymbol{\theta}_t) = \big(\boldsymbol{S}^\top \cdot \mathrm{Cov}(\boldsymbol{z}_t)^{-1} \cdot \boldsymbol{S} + \mathrm{Cov}(\boldsymbol{w}_t \,|\, \boldsymbol{\theta}_{t-1})^{-1}\big)^{-1}. \tag{24}$$

The MAP estimator of the wavefront sequence is thus also equal to the posterior mean, that is $\overline{\boldsymbol{x}}_{|t} = \boldsymbol{x}_{|t}$.

Finally, we have demonstrated the following recurrences (or updating rules):

$$\boldsymbol{w}_{t|t} = \boldsymbol{w}_{t|t-1} + \big(\boldsymbol{S}^\top \cdot \mathrm{Cov}(\boldsymbol{z}_t)^{-1} \cdot \boldsymbol{S} + \mathrm{Cov}(\boldsymbol{w}_t \,|\, \boldsymbol{\theta}_{t-1})^{-1}\big)^{-1} \cdot \boldsymbol{S}^\top \cdot \mathrm{Cov}(\boldsymbol{z}_t)^{-1} \cdot \big(\boldsymbol{y}_t - \boldsymbol{S} \cdot \boldsymbol{w}_{t|t-1}\big), \tag{25}$$

$$\mathrm{Cov}(\boldsymbol{w}_t \,|\, \boldsymbol{\theta}_t)^{-1} = \mathrm{Cov}(\boldsymbol{w}_t \,|\, \boldsymbol{\theta}_{t-1})^{-1} + \boldsymbol{S}^\top \cdot \mathrm{Cov}(\boldsymbol{z}_t)^{-1} \cdot \boldsymbol{S}, \tag{26}$$

$$\boldsymbol{x}_{|t} = \boldsymbol{x}_{|t-1} + \boldsymbol{A}_{t|t-1} \cdot \big(\boldsymbol{w}_{t|t} - \boldsymbol{w}_{t|t-1}\big), \tag{27}$$

where $\boldsymbol{A}_{t|t-1} \overset{\text{def}}{=} \mathrm{Cov}(\boldsymbol{x} \,|\, \boldsymbol{\theta}_{t-1}) \cdot \boldsymbol{Q}_{t|t-1}^\top$ has the following block structure:

$$\boldsymbol{A}_{t|t-1} = \begin{pmatrix} \vdots \\ \boldsymbol{B}_{t-2,t|t-1} \\ \boldsymbol{B}_{t-1,t|t-1} \\ \boldsymbol{I} \\ \boldsymbol{B}_{t+1,t|t-1} \\ \boldsymbol{B}_{t+2,t|t-1} \\ \vdots \end{pmatrix} \quad \text{with} \quad \boldsymbol{B}_{t',t|t-1} \overset{\text{def}}{=} \mathrm{Cov}(\boldsymbol{w}_{t'}, \boldsymbol{w}_t \,|\, \boldsymbol{\theta}_{t-1}) \cdot \mathrm{Cov}(\boldsymbol{w}_t \,|\, \boldsymbol{\theta}_{t-1})^{-1}, \tag{28}$$

where:

$$\mathrm{Cov}(\boldsymbol{w}_{t'}, \boldsymbol{w}_t \,|\, \boldsymbol{\theta}_{t-1}) \overset{\text{def}}{=} \langle (\boldsymbol{w}_{t'} - \langle \boldsymbol{w}_{t'} \,|\, \boldsymbol{\theta}_{t-1} \rangle) \cdot (\boldsymbol{w}_t - \langle \boldsymbol{w}_t \,|\, \boldsymbol{\theta}_{t-1} \rangle)^\top \,|\, \boldsymbol{\theta}_{t-1} \rangle. \tag{29}$$

The matrix $\boldsymbol{B}_{t',t|t-1}$ encodes the cross-temporal correlation between wavefronts at times t' and t knowing information up to time $t-1$. The updating rules in Eqs. (25), (26) and (27) assume that the variables (wavefront $\boldsymbol{w}_t$ and noise $\boldsymbol{z}_t$ for any frame t) are Gaussian, that the noise is centered, that the noise and the wavefront are independent, and that the noise terms in different frames are mutually independent.

To close the recurrence, the updating of the wavefront covariance leading to $\mathrm{Cov}(\boldsymbol{w}_{t+1} \,|\, \boldsymbol{\theta}_t)$ is required. This can be obtained from the updating of the statistics of $\boldsymbol{x}$ resulting from the updating of $\boldsymbol{x}$ in Eq. (27).

Remark that while the first rule in Eq. (25) is only focused on the updating of the t-th wavefront, Eq. (26) shows that the *a posteriori* covariance of the estimated t-th wavefront is reduced, hence that information has been gained, and last rule in Eq. (27) propagates this gain in information to all other frames. In particular, Eq. (27) yields the wavefront estimate $\boldsymbol{w}_{t+1|t}$ that will be needed in the next round, that is for frame $t+1$, of Eqs. (25) and (27). Hence Eqs. (25), (26) and (27), implement a complete recurrence for updating *complete statistics* of the unknowns as data arrive. In fact these equations can be seen as an instance of the well known *Kalman filter*[8] for the case of an AO system. The variables $\boldsymbol{x}$ and the tall matrix $\boldsymbol{A}_{t|t-1}$ are the analogous of the so-called *state variables* and *state transition matrix* of the Kalman filter.

Taking the $t+\delta t$-th wavefront in $\boldsymbol{x}_{|t}$ yields an updating rule for $\overline{\boldsymbol{w}}_{t+\delta t|t} = \boldsymbol{w}_{t+\delta t|t}$ the predicted wavefront required in Eq. (3):

$$\boldsymbol{w}_{t+\delta t|t} = \boldsymbol{w}_{t+\delta t|t-1} + \boldsymbol{B}_{t+\delta t,t|t-1} \cdot (\boldsymbol{w}_{t|t} - \boldsymbol{w}_{t|t-1}) \tag{30}$$

which require to solve the MAP problem in Eq. (25). How this is implemented in the actual RTC of the Themis AO system is detailed in the next section.

There are several issues for applying the proposed recursion:

(i) The updating rules do not specify how to initiate the recurrence.

(ii) The updating rules do not specify how to derive the cross-temporal covariances $\mathrm{Cov}(\boldsymbol{w}_{t'}, \boldsymbol{w}_t \,|\, \boldsymbol{\theta}_{t-1})$. These terms may be learned from the available data but this certainly requires some assumptions on their structure.

(iii) In practice, we must work with a truncated sequence, not the virtually infinite sequence $\boldsymbol{x}$ considered so far. Owing to the recursive structure of the equations, $\boldsymbol{x}$ shall be implemented as a sliding temporal window of given length.

(iv) All necessary computations must be carried out faster than the rate of the AO system loop. Typically in less than 1 ms at 1 kHz for the Themis AO system.

2.5 Comparison with Conventional AO Systems

In a simple conventional AO system, the new commands are assumed given by:

$$\boldsymbol{a}_{t+\delta t} = \boldsymbol{a}_t - \gamma\, \boldsymbol{G}^\ddagger \cdot \boldsymbol{d}_t \tag{31}$$

with $\boldsymbol{a}_t$ the commands at time t, $\boldsymbol{G}^\ddagger \approx \boldsymbol{G}^\dagger$ the WFS data to DM commands matrix which is an approximation of $\boldsymbol{G}^\dagger = \left(\boldsymbol{G}^\top \cdot \boldsymbol{G}\right)^{-1} \cdot \boldsymbol{G}^\top$ the pseudo inverse of the interaction matrix $\boldsymbol{G}$, and $\gamma \in (0, 1]$ the control loop gain. To achieve a certain level of regularization, $\boldsymbol{G}^\ddagger$ is usually a truncated SVD version of $\boldsymbol{G}^\dagger$.

Dropping the prediction in the optimal control and directly expressing the wavefront in the basis of the influence functions of the deformable mirror amounts to using the commands $\boldsymbol{a}_{t+\delta t} = -\boldsymbol{w}_{t|t}$ with $\boldsymbol{w}_{t|t}$ the MAP wavefront estimator given in Eq. (25). Then the commands are given by:

$$\begin{aligned} \boldsymbol{a}_{t+\delta t} &= \boldsymbol{a}_t - \left(\boldsymbol{S}^\top \cdot \mathrm{Cov}(\boldsymbol{z}_t)^{-1} \cdot \boldsymbol{S} + \mathrm{Cov}(\boldsymbol{w}_t \,|\, \boldsymbol{\theta}_{t-1})^{-1}\right)^{-1} \cdot \boldsymbol{S}^\top \cdot \mathrm{Cov}(\boldsymbol{z}_t)^{-1} \cdot \left(\boldsymbol{y}_t + \boldsymbol{S} \cdot \boldsymbol{a}_t\right) \\ &= \boldsymbol{a}_t - \left(\boldsymbol{G}^\top \cdot \mathrm{Cov}(\boldsymbol{z}_t)^{-1} \cdot \boldsymbol{G} + \mathrm{Cov}(\boldsymbol{w}_t \,|\, \boldsymbol{\theta}_{t-1})^{-1}\right)^{-1} \cdot \boldsymbol{G}^\top \cdot \mathrm{Cov}(\boldsymbol{z}_t)^{-1} \cdot \boldsymbol{d}_t, \end{aligned} \tag{32}$$

since $\boldsymbol{S} = \boldsymbol{G}$ in that case and thus $\boldsymbol{y}_t + \boldsymbol{S}\cdot\boldsymbol{a}_t = \boldsymbol{y}_t + \boldsymbol{G}\cdot\boldsymbol{a}_{t-1} = \boldsymbol{d}_t$. Even though:

Note the analogies between Eqs. (31) and (32). The two approaches are equivalent provided:

$$\gamma\,\boldsymbol{G}^{\ddagger} \approx \left(\boldsymbol{G}^\top\cdot\mathrm{Cov}(\boldsymbol{z}_t)^{-1}\cdot\boldsymbol{G} + \mathrm{Cov}(\boldsymbol{w}_t\,|\,\boldsymbol{\theta}_{t-1})^{-1}\right)^{-1}\cdot\boldsymbol{G}^\top\cdot\mathrm{Cov}(\boldsymbol{z}_t)^{-1} \tag{33}$$

holds to a sufficient precision.

2.6 The Commands in the Current Themis AO System

In the first version of the Themis AO system, we chose to simplify the computations so that they remain compatible with a real-time system running on a conventional CPU and so that they can be controlled with a very small number of parameters (not all the statistics). To that end, when solving the MAP problem in Eq. (25), we approximate the wavefront regularization by:

$$\left\|\boldsymbol{w}_t - \boldsymbol{w}_{t|t-1}\right\|^2_{\mathrm{Cov}(\boldsymbol{w}_t\,|\,\boldsymbol{\theta}_{t-1})^{-1}} \approx \mu_t\left\|\boldsymbol{w}_t\right\|^2_{\boldsymbol{C}^{-1}} + \rho_t\left\|\boldsymbol{w}_t - \boldsymbol{w}_{t-1|t-1}\right\|^2 \tag{34}$$

where $\boldsymbol{C}$ is the covariance matrix for a Kolmogorov wavefront with a given diameter over Fried's parameter D/r_0 ratio. The first term in the above penalty imposes spatial regularization of the wavefront, the hyper-parameter $\mu_t \propto (D/r_0)^{-5/3}$ has to be tuned according to the strength of the turbulence. The second regularization term imposes the temporal continuity of the wavefront. The estimated MAP wavefront at time t is then given by:

$$\begin{aligned}\boldsymbol{w}_{t|t} &= \arg\min_{\boldsymbol{w}_t}\left\{\left\|\boldsymbol{y}_t - \boldsymbol{S}\cdot\boldsymbol{w}_t\right\|^2_{\mathrm{Cov}(\boldsymbol{z}_t)^{-1}} + \mu_t\left\|\boldsymbol{w}_t\right\|^2_{\boldsymbol{C}^{-1}} + \rho_t\left\|\boldsymbol{w}_t - \boldsymbol{w}_{t-1|t-1}\right\|^2\right\}\\ &= \left(\boldsymbol{S}^\top\cdot\mathrm{Cov}(\boldsymbol{z}_t)^{-1}\cdot\boldsymbol{S} + \mu_t\,\boldsymbol{C}^{-1} + \rho_t\,\boldsymbol{I}\right)^{-1}\cdot\left(\boldsymbol{S}^\top\cdot\mathrm{Cov}(\boldsymbol{z}_t)^{-1}\cdot\boldsymbol{y}_t + \rho_t\,\boldsymbol{w}_{t-1|t-1}\right),\end{aligned} \tag{35}$$

where the pseudo open-loop data $\boldsymbol{y}_t$ are given by Eq. (4).

Unrelated to our simplifying assumptions, an important consequence of the MAP approach is that while the commands linearly depend on the wavefront sensor data, the corresponding matrix:

$$\left(\boldsymbol{G}^\top\cdot\mathrm{Cov}(\boldsymbol{z}_t)^{-1}\cdot\boldsymbol{G} + \mu_t\,\boldsymbol{W} + \rho_t\,\boldsymbol{I}\right)^{-1}\cdot\boldsymbol{G}^\top\cdot\mathrm{Cov}(\boldsymbol{z}_t)^{-1} \tag{36}$$

cannot be computed once for all since it depends on the time. In other words the control law changes with time which is an important feature to cope with variable observing conditions.

Measurements from different sub-pupils can be considered as independent so the noise covariance matrix $\mathrm{Cov}(\boldsymbol{z}_t)$ has a block-diagonal structure with 2×2 blocks[‡]. Each block accounts for the variances of the horizontal and vertical slopes and for their covariance. The measurements $\boldsymbol{d}_t$ and their covariances are estimated by the real-time data processing software of the wavefront sensor (see proceedings by Tallon *et al.* in this conference[5]). Owing to its block diagonal structure, the noise covariance matrix $\mathrm{Cov}(\boldsymbol{z}_t)$ is very sparse. The linear response matrix $\boldsymbol{S}$ of a Shack-Hartmann wavefront sensor is also very sparse. With such sparse matrices, the solution $\boldsymbol{w}_{t|t}$ can be computed iteratively by means of the FRiM method[1] taking $\boldsymbol{C} = \boldsymbol{K}\cdot\boldsymbol{K}^\top$ with $\boldsymbol{K}$ the *fractal operator* of FRiM.

To further speedup computations, we consider working directly with the wavefronts represented on the basis of the deformable mirror influence functions and with no prediction. This amounts to taking $\boldsymbol{M} = \boldsymbol{I}$ and $\delta t = 0$ in Eq. (3) and to taking $\boldsymbol{S} = \boldsymbol{G}$ in all other equations. The control commands are then given by:

$$\begin{aligned}\boldsymbol{a}_{t+\delta t} &= \arg\min_{\boldsymbol{a}}\left\{\left\|\boldsymbol{y}_t + \boldsymbol{G}\cdot\boldsymbol{a}\right\|^2_{\mathrm{Cov}(\boldsymbol{z}_t)^{-1}} + \mu_t\left\|\boldsymbol{a}\right\|^2_{\boldsymbol{W}} + \rho_t\left\|\boldsymbol{a} - \boldsymbol{a}_t\right\|^2\right\}\\ &= \left(\boldsymbol{G}^\top\cdot\mathrm{Cov}(\boldsymbol{z}_t)^{-1}\cdot\boldsymbol{G} + \mu_t\,\boldsymbol{W} + \rho_t\,\boldsymbol{I}\right)^{-1}\cdot\left(\rho_t\,\boldsymbol{a}_t - \boldsymbol{G}^\top\cdot\mathrm{Cov}(\boldsymbol{z}_t)^{-1}\cdot\boldsymbol{y}_t\right),\end{aligned} \tag{37}$$

where the pseudo open-loop data $\boldsymbol{y}_t$ are given by Eq. (4) and where $\boldsymbol{W}$ is the inverse of the *a priori* spatial covariance of the commands. The *a priori* precision matrix $\boldsymbol{W}$ can be based on Kolmogorov statistics but for the actuators.

[‡]provided horizontal and vertical measured slopes are contiguous in the data vector $\boldsymbol{d}_t$

To compare our commands with the ones assumed in simple conventional AO systems, and given in Eq. (31), and to the ones in Eq. (32), our control commands can be put in the form of an updating of the previous commands involving the wavefront sensor data $\boldsymbol{d}_t$ instead of the POL data $\boldsymbol{y}_t$:

$$\begin{aligned}\boldsymbol{a}_{t+\delta t} = \boldsymbol{a}_t &- \left(\boldsymbol{G}^\top \cdot \mathrm{Cov}(\boldsymbol{z}_t)^{-1} \cdot \boldsymbol{G} + \mu_t\, \boldsymbol{W} + \rho_t\, \boldsymbol{I}\right)^{-1} \cdot \boldsymbol{G}^\top \cdot \mathrm{Cov}(\boldsymbol{z}_t)^{-1} \cdot \boldsymbol{d}_t \\ &- \mu_t \left(\boldsymbol{G}^\top \cdot \mathrm{Cov}(\boldsymbol{z}_t)^{-1} \cdot \boldsymbol{G} + \mu_t\, \boldsymbol{W} + \rho_t\, \boldsymbol{I}\right)^{-1} \cdot \boldsymbol{W} \cdot \boldsymbol{a}_t. \end{aligned} \tag{38}$$

3. CALIBRATIONS

The optimal control of an AO system relies on the assumed models of the wavefront sensor, of the deformable mirror, and of the statistics of the wavefront and of the noise. The components of the model of the system have to be carefully calibrated. We exploit the fact that the AO system includes a measuring device (the wavefront sensor) and means to modify the system (the deformable mirror) to perform these calibrations with the AO system itself.

3.1 Detector Calibration and Image Pre-Processing

The calibration of the detector of the wavefront sensor is fully described in the proceedings by Tallon *et al.* in this conference.[5] In a nutshell, this calibration provides 4 pre-processing parameters per pixel. Two of these parameters implement an affine pixel-wise correction to compensate for the non-uniform bias and overall sensitivity of the detector. The two other parameters are needed to estimate the non-uniform precision (reciprocal of the variance) of the pixels in each pre-processed image.

In the RTC of the Themis AO system (see Section 4), a *camera server* is continuously acquiring raw images from the wavefront sensor camera. As soon as a new raw image is available, the camera server applies the pre-processing and delivers the pre-processed image and the corresponding pixel precisions to other processes via shared memory.

3.2 Live Calibration of the Interaction Matrix

The interaction matrix $\boldsymbol{G} = \boldsymbol{S} \cdot \boldsymbol{M}$ encodes the linear relationship between the actuator commands and the wavefront sensor data. In order to calibrate this matrix, we register data frames of the wavefront sensor with perturbed commands and given by:

$$\boldsymbol{d}_t = \boldsymbol{S} \cdot (\boldsymbol{w}_t + \boldsymbol{M} \cdot (\boldsymbol{a}_t + \varepsilon\, \boldsymbol{u}_t)) + \boldsymbol{z}_t \tag{39}$$

with $\boldsymbol{u}_t \in \mathbb{R}^{n_{\mathrm{act}}}$ a known vector of random perturbation and $\varepsilon > 0$ the strength of the perturbation. The random perturbations are centered, $\langle \boldsymbol{u}_t \rangle = \boldsymbol{0}$, mutually independent and identically distributed (i.i.d.) with a known covariance $\boldsymbol{U} = \mathrm{Cov}(\boldsymbol{u}_t) = \langle \boldsymbol{u}_t \cdot \boldsymbol{u}_t^\top \rangle$.

We then form the following mean cross-product:

$$\widehat{\boldsymbol{V}} = \frac{1}{n\,\varepsilon} \sum_{t=1}^{n} \boldsymbol{d}_t \cdot \boldsymbol{u}_t^\top \tag{40}$$

whose expectation is given by:

$$\begin{aligned}\left\langle \widehat{\boldsymbol{V}} \right\rangle &= \frac{1}{n\,\varepsilon} \sum_{t=1}^{n} \left\{ \boldsymbol{S} \cdot \left(\langle \boldsymbol{w}_t \cdot \boldsymbol{u}_t^\top \rangle - \boldsymbol{M} \cdot \langle \boldsymbol{a}_t \cdot \boldsymbol{u}_t^\top \rangle + \varepsilon\, \boldsymbol{M} \cdot \langle \boldsymbol{u}_t \cdot \boldsymbol{u}_t^\top \rangle \right) + \langle \boldsymbol{z}_t \cdot \boldsymbol{u}_t^\top \rangle \right\} \\ &= \frac{1}{n\,\varepsilon} \sum_{t=1}^{n} \left\{ \boldsymbol{S} \cdot \left(\langle \boldsymbol{w}_t \rangle \cdot \langle \boldsymbol{u}_t^\top \rangle - \boldsymbol{M} \cdot \langle \boldsymbol{a}_t \rangle \cdot \langle \boldsymbol{u}_t \rangle^\top + \varepsilon\, \boldsymbol{M} \cdot \langle \boldsymbol{u}_t \cdot \boldsymbol{u}_t^\top \rangle \right) + \langle \boldsymbol{z}_t \rangle \cdot \langle \boldsymbol{u}_t \rangle^\top \right\} \\ &= \frac{1}{n}\, \boldsymbol{S} \cdot \boldsymbol{M} \cdot \sum_{t=1}^{n} \langle \boldsymbol{u}_t \cdot \boldsymbol{u}_t^\top \rangle = \boldsymbol{G} \cdot \boldsymbol{U} \end{aligned} \tag{41}$$

where the first right-and-side (RHS) comes from Eq. (39) and from the linearity of the expectation, the second RHS follows from the independence of $\boldsymbol{u}_t$ with all other variables, and the third RHS from the fact that the perturbations are centered, *i.e.* $\langle \boldsymbol{u}_t \rangle = \boldsymbol{0}$, and i.i.d., thus $\langle \boldsymbol{u}_t \cdot \boldsymbol{u}_t^\top \rangle = \mathrm{Cov}(\boldsymbol{u}_t) = \boldsymbol{U}$ for all t, and finally using $\boldsymbol{G} = \boldsymbol{S} \cdot \boldsymbol{M}$.

An *unbiased estimator* of the influence matrix is thus:

$$\widehat{\boldsymbol{G}} = \widehat{\boldsymbol{V}} \cdot \boldsymbol{U}^{-1} \tag{42}$$

with $\boldsymbol{U}$ the exact covariance matrix of the perturbations. For the sake of simplicity, the perturbations $\boldsymbol{u}_t$ may be chosen so that their covariance matrix is the identity matrix: $\boldsymbol{U} = \boldsymbol{I}$.

An advantage of this calibration method is that it can be carried out while the AO system is running. Indeed, thanks to the fact that the perturbations are centered and independent to any other variables, the influences of the turbulent wavefront $\boldsymbol{w}_t$, of the actuators commands $\boldsymbol{a}_t$, and of the measurement noise $\boldsymbol{z}_t$ cancel on average in $\widehat{\boldsymbol{V}}$. The only restriction is to choose the strength ε of the perturbation not too high to not destroy the correction[§] and yet high enough to have a measurable incidence in the wavefront sensor data $\boldsymbol{d}_t$.

Since the perturbations are known, it is possible to compute the conditional expectation of $\widehat{\boldsymbol{V}}$:

$$\begin{aligned} \left\langle \widehat{\boldsymbol{V}} \,\middle|\, \{\boldsymbol{u}_t\}_{t\in 1:n} \right\rangle &= \boldsymbol{G} \cdot \widehat{\boldsymbol{U}} + \frac{1}{n\,\varepsilon} \sum_{t=1}^{n} [\boldsymbol{S} \cdot (\langle \boldsymbol{w}_t \rangle - \boldsymbol{M} \cdot \langle \boldsymbol{a}_t \rangle) + \langle \boldsymbol{z}_t \rangle] \cdot \boldsymbol{u}_t^\top \\ &= \boldsymbol{G} \cdot \widehat{\boldsymbol{U}} \end{aligned} \tag{43}$$

provided $\boldsymbol{S} \cdot (\langle \boldsymbol{w}_t \rangle - \boldsymbol{M} \cdot \langle \boldsymbol{a}_t \rangle) + \langle \boldsymbol{z}_t \rangle = 0$ holds and with:

$$\widehat{\boldsymbol{U}} = \frac{1}{n} \sum_{t=1}^{n} \boldsymbol{u}_t \cdot \boldsymbol{u}_t^\top . \tag{44}$$

This yields another estimator (which is unbiased conditionally to the knowledge of the perturbations) for the interaction matrix $\boldsymbol{G}$:

$$\widehat{\boldsymbol{G}} = \widehat{\boldsymbol{V}} \cdot \widehat{\boldsymbol{U}}^{-1} . \tag{45}$$

From preliminary tests, it seems that Eq. (45) provides a better estimator than Eq. (42).

In practice, we use a binomial law for the perturbations:

$$[\boldsymbol{u}_t]_i = \begin{cases} +1 & \text{with } 50\% \text{ probability} \\ -1 & \text{else} \end{cases} \tag{46}$$

and take ε equal to a few percents of the dynamics of the actuators. This choice yields the covariance matrix $\boldsymbol{U} = \boldsymbol{I}$. The interaction matrix $\boldsymbol{G}$ is mostly sparse because the extension of the influence functions of the deformable mirror are limited. To get rid of the noise in the entries of $\boldsymbol{G}$ of small amplitude, we only keep the most significant coefficients of each column of the interaction matrix (that is for each actuator). For that, we apply a hard thresholding on the coefficients of $\widehat{\boldsymbol{G}}$ as follows:

$$\widehat{G}_{i,j}^{\text{sparse}} = \begin{cases} \widehat{G}_{i,j} & \text{if } \sqrt{\widehat{G}_{i_\text{h}(i),j}^2 + \widehat{G}_{i_\text{v}(i),j}^2} > \max\left(\tau^{\text{abs}}, \tau^{\text{rel}} \max_{j'} \sqrt{\widehat{G}_{i_\text{h}(i),j'}^2 + \widehat{G}_{i_\text{v}(i),j'}^2}\right) \\ 0 & \text{else} \end{cases} \tag{47}$$

to where $i_\text{h}(i)$ and $i_\text{v}(i)$ yield the index of the wavefront measurement corresponding to the slopes respectively along the horizontal and vertical axes for the i-th measurement and where $\tau^{\text{abs}} \geq 0$ and $\tau^{\text{rel}} \geq 0$ are chosen absolute and relative threshold levels. Assuming 1-based indexing and that the 2 slopes measured for a given sub-image are contiguous in the data, then $i_\text{h}(i) = 2\,\lfloor (i-1)/2 \rfloor + 1$ and $i_\text{v}(i) = i_\text{h}(i) + 1$.

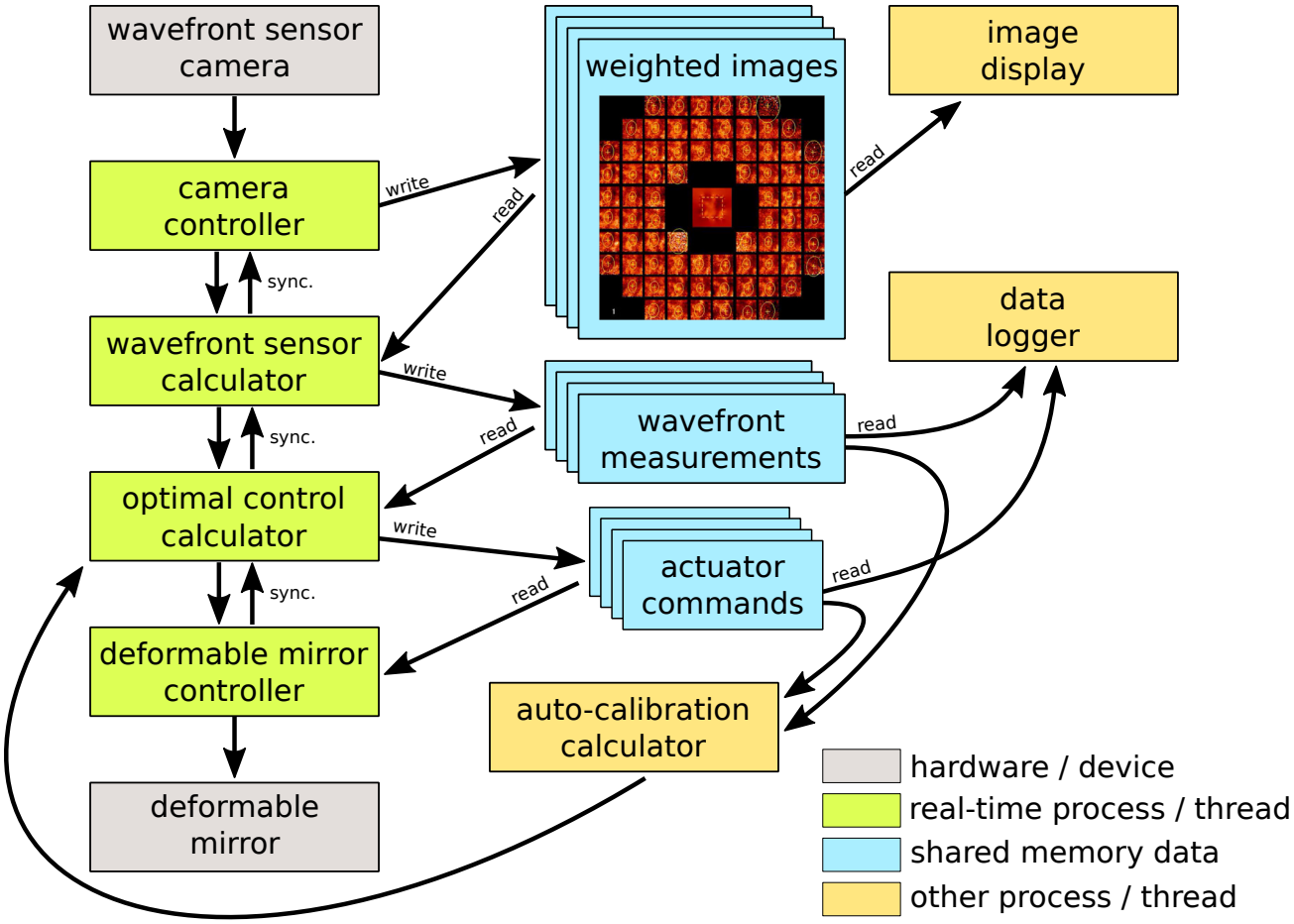

Figure 2. The RTC framework of THEMIS.

4. REAL-TIME CONTROL

The real time control (RTC) software of the THEMIS AO system runs on a Linux workstation with a 4 core i7-4790K CPU at 4.2 GHz. The Linux kernel is a *low-latency* version. The RTC of the THEMIS AO system consists in multiple processes which collaborate to execute the various tasks (see Fig. 2). The time critical processes (wavefront sensor camera sever, wavefront sensor calculator, control command calculator, and deformable mirror server) run with a real-time priority to avoid jitters and latency in their execution. Other non-critical processes (visualization, telemetry collector, statistics calculator, *etc.*) run with normal priorities. All theses processes use a common framework called TAO (which is the acronym for *a Toolkit for Adaptive Optics systems*) which is a set of libraries written in C and bindings for different languages (currently C, Julia,[9] Yorick, and Unix shell). TAO is meant to be portable and flexible. Several models of devices (cameras, deformable mirrors, LCD phase screens, and step motor controllers) have been interfaced in TAO. Most of the software is publicly available[¶].

In the TAO framework, devices (the wavefront camera and the deformable mirror) are managed by servers:

- The server owning the **wavefront camera** continuously acquires images as quickly as possible, applies image pre-processing (affine correction and estimation of the pixel-wise precision) and delivers the resulting *weighted images* via shared memory to other processes. Shared read/write locks and condition variables are used to notify the other processes that a new image is available.

[§]since the perturbations are known, their impact in the wavefront sensor measurements can be removed provided that the influence matrix $\boldsymbol{G}$ is known with sufficient accuracy

[¶]https://git-cral.univ-lyon1.fr/tao

- The server owning the **deformable mirror** (DM) may receive actuators commands from any other process and apply these commands to the DM accounting for given reference commands preset so as to compensate for non common path aberrations (NCPA). The server stores in shared memory a cyclic history of the commands effectively applied to the DM (taking into account the reference and limitations of the DM such as minimal and maximal command levels). This history is updated immediately after applying the commands and other processes are notified so that they can figure out exactly which commands have been sent. This is needed, in particular, to compute the pseudo open-loop data.

The servers share information and receive commands from other processes via resources stored in shared memory and whose access is controlled by shared read/write locks and condition variables. With critical processes ran with real-time priority, the latency between a condition being notified and the process waiting for this condition to be awaken is small and quite stable (about $6 \pm 1\,\mu s$). Latency of the same order have been measured for other RTC software like CACAO[10] relying on semaphores for process synchronization. We chose read/write locks and conditions variables so as to be the most flexible regarding which clients are allowed to connect to which resources and we rely on real-time priorities and the Linux process scheduler to dispatch the available CPU power. Compared to semaphores, read/write locks (like mutexes) may result in dead-locks if incorrectly used.

There are several advantages in the splitting of the tasks among several processes and in the sharing of information in shared memory:

- There are no latency due to transferring/copying of data.
- The available CPU power is better exploited and the latency reduced (in spite of the small delays induced by process synchronization) because a process can deliver the result of its work to others as soon as possible and then executes post-processing tasks.
- Non-sequential coding is more appropriate for implementing an AO system RTC and it turns out that the resulting code is considerably simpler than an equivalent version implemented with sequential coding.
- Once a device server is launched, any other process have access to the device and there is no restrictions on the number of clients accessing a given resources.

Accounting for the synchronization of tasks, THEMIS AO RTC is able to send commands to the deformable mirror with a delay of $\simeq 220\,\mu s$ after receiving the raw image from the wavefront sensor camera (see Fig. 3). The RTC was tested with a loop frequency up to 1.2 kHz.

5. FIRST CLOSING OF THE LOOP AND FIRST IMAGES

We closed the loop for the first time on the 8th of December 2020. Figures 4–6 show some images of the Sun in open and closed loop at that time[‖]. Figure 7 shows the benefits of the AO system but also of the post-processing of images acquired in closed loop (here by a Knox-Thompson method). Figures 9 and 8 show the results obtained by post-processing images recently acquired in closed loop with the THEMIS AO system in March and April 2022. These images demonstrate the great potential of this instrument (the fine grains seen between the granules are caused by small scale structures of the magnetic field and have a size of about 0.2" which is close to the diffraction limit of THEMIS).

ACKNOWLEDGMENTS

The project has been funded through the FP7 program INFRA-2012-1.1.26, SOLARNET grant agreement n° 312495 of the European Commission. It has also obtained support from the "*Action Spécifique Haute Résolution Angulaire*" (ASHRA) of CNRS-INSU co-funded by CNES and the Actions Incitatives of the "*Centre de Recherches Astrophysiques de Lyon*" (CRAL).

[‖]For more details and movies, see https://git-cral.univ-lyon1.fr/isabelle.tallon-bosc/tao-news/ and http://161.72.34.10/dokuwiki/doku.php?id=themis_ao_first_light.

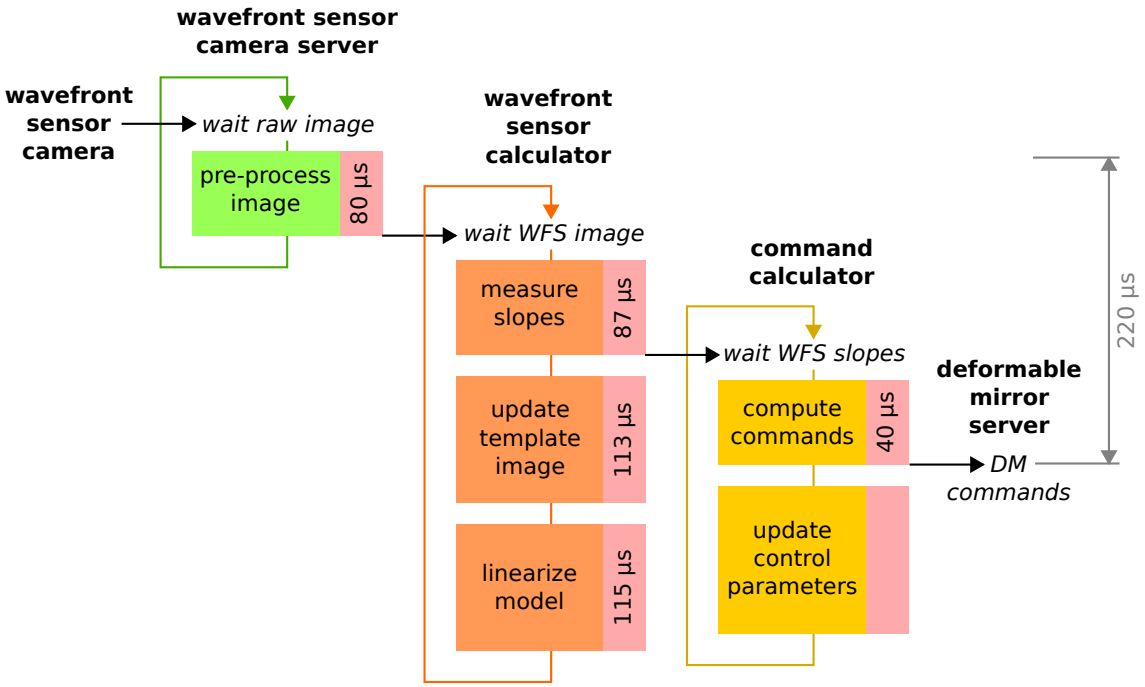

Figure 3. Scheduling of real-time tasks in THEMIS AO control. The RTC is able to deliver deformable mirros commands with a delay of $\simeq 220\,\mu s$ from the acquisition of the raw wavefront sensor image

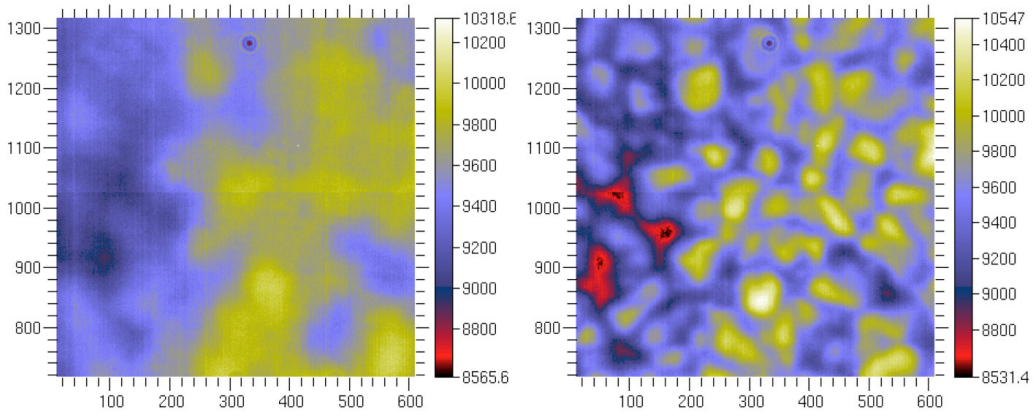

Figure 4. First closing of the loop (8 December 2020). Images of a 14.6" field of view (FOV) of the Sun in a H_α filter and centered at the FOV of the wavefront sensor. Left: open loop. Right: closed loop at 1 kHz. Temporal smoothing of 0.5 s, Fried's parameter estimated to be $r_0 \simeq 5\,cm$.

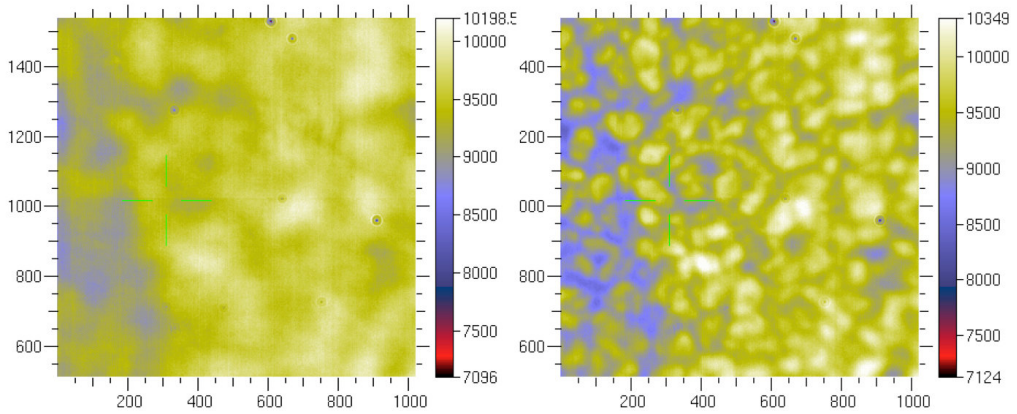

Figure 5. Same as Fig. 4 but for a larger FOV of 25" and in worse turbulence conditions: Fried's parameter estimated to be $r_0 \simeq 3\,\mathrm{cm}$. The green cross indicates the center of the wavefront sensor 10" FOV.

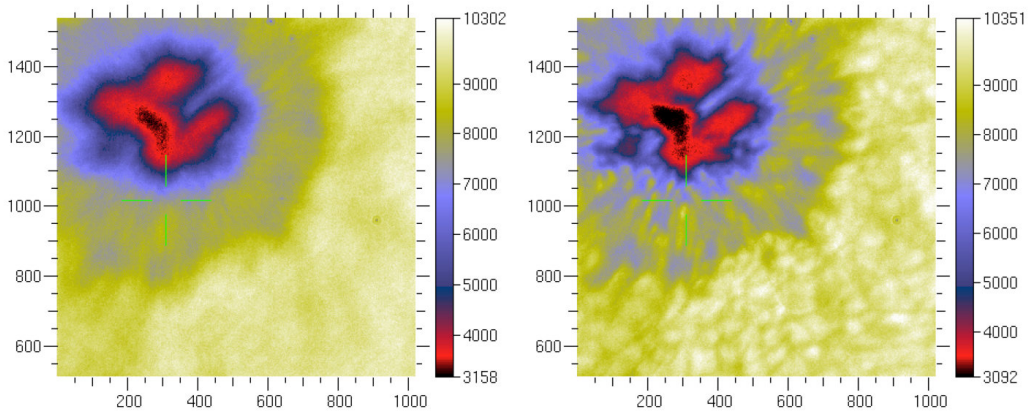

Figure 6. Sun spot observed on 8th of December 2020. Left: open loop. Right: closed loop at 1 kHz. 25" FOV. The green cross indicates the center of the wavefront sensor 10" FOV.

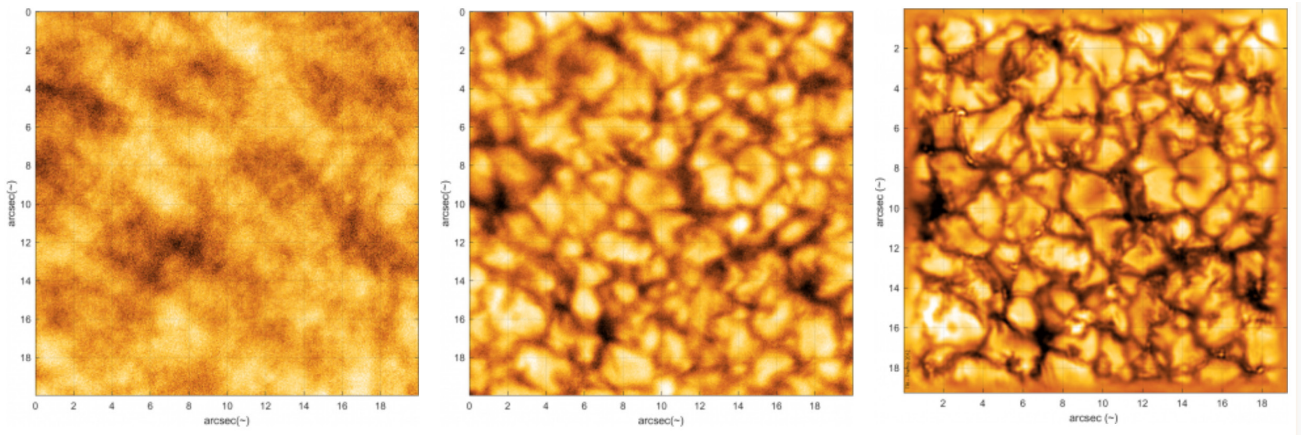

Figure 7. Solar granulation observed with THEMIS AO system. Left: open loop, granulation contrast: 1.7 %. Middle: closed loop, granulation contrast: 4.2 %. Right: result of post-processing of 100 images in closed loop (Knox-Thompson), granulation contrast: 9.6 %. Fried's parameter estimated to be $r_0 \simeq 3 - 4\,\mathrm{cm}$.

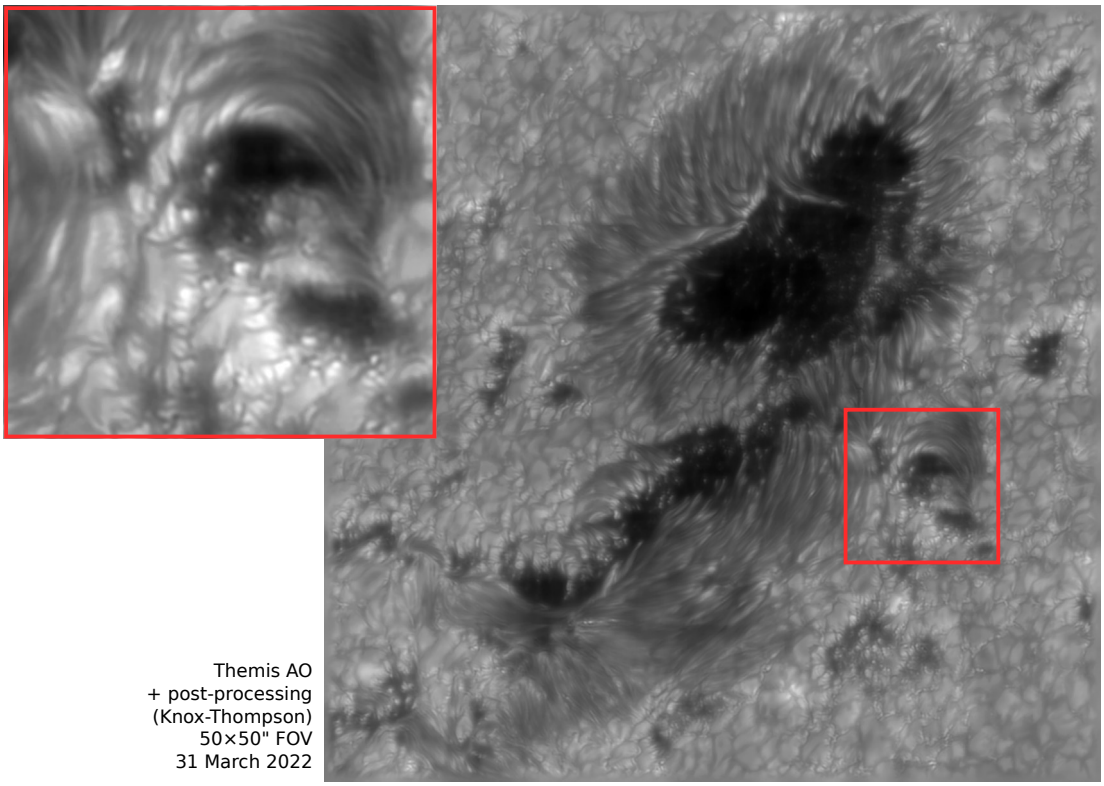

Figure 8. Sun spots with THEMIS AO system and post-processed of images in closed loop.

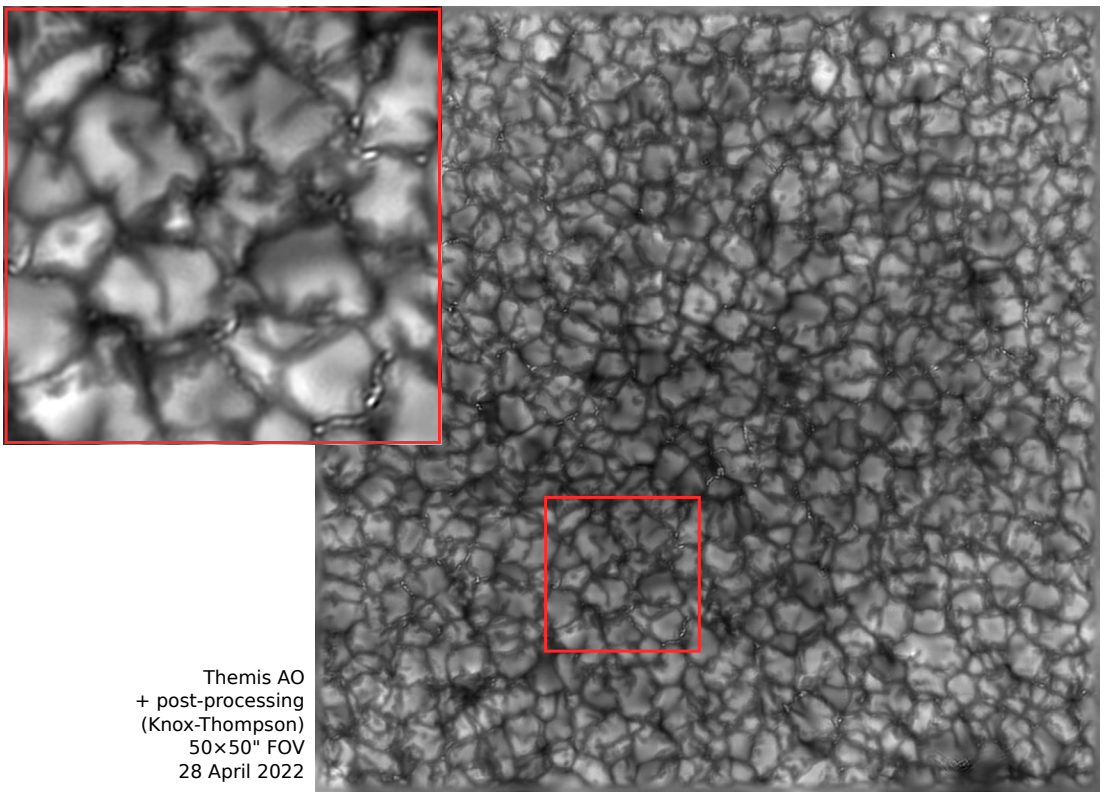

Figure 9. Solar granulation with THEMIS AO system and post-processed of images in closed loop.

REFERENCES

[1] Thiébaut, É. and Tallon, M., "Fast minimum variance wavefront reconstruction for extremely large telescopes," *J. Opt. Soc. Am. A* **27**(5), 1046–1059 (2010).

[2] Béchet, C., Tallon, M., and Thiébaut, É., "Comparison of minimum-norm maximum likelihood and maximum a posteriori wavefront reconstructions for large adaptive optics systems," *J. Opt. Soc. Am. A* **26**(3), 497–508 (2009).

[3] Béchet, C., Tallon, M., and Thiébaut, É., "Optimization of adaptive optics correction during observations: Algorithms and system parameters identification in closed-loop," in [*SPIE Astronomical Telescopes and Instrumentation*], 84472C, International Society for Optics and Photonics (Sept. 2012).

[4] Thiébaut, É., Tallon, M., Denis, L., Langlois, M., Béchet, C., Moretto, G., and Gelly, B., "Innovative real-time processing for solar adaptive optics," in [*SPIE Astronomical Telescopes and Instrumentation, Adaptive Optics Systems VI*], **10703**, 107031I, International Society for Optics and Photonics (2018).

[5] Tallon, M., Thiébaut, E., Tallon-Bosc, I., Gelly, B., and Denis, L., "Solar wavefront sensing at themis with self-calibrated reference image and estimation of the noise covariance," in [*SPIE Astronomical Telescopes and Instrumentation*], 12185–91, International Society for Optics and Photonics (July 2022).

[6] Gilles, L., "Closed-loop stability and performance analysis of least-squares and minimum-variance control algorithms for multiconjugate adaptive optics," *Applied Optics* **44**(6), 993–1002 (2005).

[7] Tarantola, A., [*Inverse Problem Theory*], Elsevier (1987).

[8] Kalman, R. E., "A new approach to linear filtering and prediction problems," *Journal of basic Engineering* **82**(1), 35–45 (1960).

[9] Bezanson, J., Edelman, A., Karpinski, S., and Shah, V. B., "Julia: A fresh approach to numerical computing," *SIAM Review* **59**, 65–98 (jan 2017).

[10] Guyon, O., Sevin, A., Ferreira, F., Ltaief, H., Males, J., Deo, V., Gratadour, D., Cetre, S., Martinache, F., Lozi, J., Vievard, S., Fruitwala, N., Bos, S., and Skaf, N., "Adaptive optics real-time control with the compute and control for adaptive optics (cacao) software framework," in [*SPIE Astronomical Telescopes and Instrumentation*], **11448**, 114482N, International Society for Optics and Photonics (2020).